IEEE Access
Multidisciplinary ⋮ Rapid Review ⋮ Open Access Journal

Received March 28, 2021, accepted April 9, 2021, date of publication April 13, 2021, date of current version April 23, 2021.

Digital Object Identifier 10.1109/ACCESS.2021.3073004

Performance Improvement of Three-Phase Boost Power Factor Correction Rectifier Through Combined Parameters Optimization of Proportional-Integral and Repetitive Controller

MUHAMMAD SAQIB ALI[1,2], LEI WANG[1], HANI ALQUHAYZ[3], OBAID UR REHMAN[2], AND GUOZHU CHEN[1], (Member, IEEE)

[1]College of Electrical and Engineering, Institute of Power Electronics, Zhejiang University, Hangzhou 310027, China
[2]Department of Electrical and Computer Engineering, COMSATS University Islamabad (CUI), Islamabad 45550, Pakistan
[3]Department of Computer Science and Information, College of Science in Zulfi, Majmaah University, Al-Majmaah 11952, Saudi Arabia

Corresponding authors: Muhammad Saqib Ali (msaqibali@zju.edu.cn) and Guozhu Chen (gzchen@zju.edu.cn)

This work was supported by the National Natural Foundation of China under Grant 51777186.

ABSTRACT This paper performs parameter optimization of proportional-integral (PI) and repetitive controller (RC) with a new objective function by adding two degrees of freedom for a three-phase boost power factor correction (PFC) rectifier. The main objectives are to optimize the multiple control loop parameters for total harmonics distortion (THD) reduction and dynamic performance indices improvement, including overshoot, rise time, and zero steady-state error. The control parameters of the three-phase boost PFC rectifier are optimized through a standard genetic algorithm. After obtaining the optimal PI and RC parameters values, fast Fourier transform and dynamic response analysis were performed using MATLAB. Moreover, separate evaluation functions are used to validate the optimal results in terms of THD reduction and dynamic performance indices improvement. Furthermore, the results are compared with the existing objective functions to show the proposed objective function superiority. Simulation results demonstrated that our proposed objective function outperforms existing objective functions to achieve optimal PI and RC parameters value. Finally, simulation results are validated through experimental results. The experimental setup includes a 5kW three-phase PFC rectifier with DSP TMS320F28335 prototype hardware to verify controller parameter performance.

INDEX TERMS Genetic algorithm, PI control, repetitive controller, ZLG objective function, degree of freedom, power factor correction, total harmonics distortion.

I. INTRODUCTION

The widespread use of the active AC-DC rectifier leads to the rise in non-linearity of electronic equipment resulting in grid current degradation. Therefore, to handle such a problem efficiently, a three-phase boost power factor correction (PFC) rectifier has gained further popularity [1]–[5]. The performance of three-phase boost PFC rectifier in terms of unity power factor (PF), total harmonics distortion (THD) reduction and dynamic performance indices improvement such as overshoot (M_p), settling time (t_s), rise time (t_r) and steady-state error (E_{ss}) can be significantly improved by adopting efficient controller strategies. The control strategies are categorized as: (1) intelligent control (2) conventional control. Adaptive, predictive, and fuzzy controllers lie in intelligent controls [6]–[9]. Recent development in digital technology accelerates the use of intelligent control in PFC rectifiers; however, it results in more calculation complexity and computation burden on the regular processor. On the other hand, most commonly used conventional control strategies such as PI controller have improved the three-phase PFC rectifier performance tremendously due to its simple structure and robust design [10]–[14]. Therefore, PI control is still the easiest and most feasible controller in a wide range of operating conditions and consumes more than 90 percent of the control algorithm [15], [16].

The associate editor coordinating the review of this manuscript and approving it for publication was Cheng Qian.

Two control loops are mainly existing in the three-phase boost PFC rectifier control configurations: (1) Inner active and reactive current control (2) Outer DC voltage control to retain stable DC-link voltage under unbalanced and distorted voltage conditions [17], [18]. It is worth noting that the PI controller is not sufficient for the inner current loop to suppress the THD, particularly 5^{th} and 7^{th} order harmonics. Therefore, PI controller needs to be combined with some other control techniques, like repetitive control (RC) [19]–[23]. However, it increases the design complexity due to multi-control loops, which can hardly be handled with conventional design methods [24]. Therefore, an optimization approach for multiple control loops based on a discrete transfer function is required for the controller parameters reliable and practical implementation.

For tuning and determining the gains of PID controllers, several empirical strategies such as Ziegler-Nichols (ZN) and Cohen-Coon have been proposed [25], [26]. However, it is often hard to tune PID parameters using these strategies due to the oscillatory set-point responses, substantial time delay, and hence may not produce satisfactory closed-loop responses. For such reasons, empirical strategies do not yield optimal results. These issues are effectively tackled in literature with nature-inspired algorithms. For instance, genetic algorithm (GA) [27]–[32] and particle swarm optimization (PSO) [33]–[37] have been successfully applied for parameter optimization in PFC and active power filter (APF) systems. The aforementioned literature addresses parameter optimization for the PFC system and mainly focuses on the PI control parameter optimization. A couple of studies suggested integrated control of PI and RC for improving harmonics suppression capability [18]–[21], however leading to multiple control loops, which makes control parameters optimization more complex.

GA is one of the widely adopted optimization approach for control parameter optimization [38]. It provides efficient solutions for parameter and system identification, mainly due to its simplified approach. Furthermore, GA has a simultaneous search method that mimics natural genetic operations; thus, GA approach is typically quicker [39]. Meanwhile, GA can effectively implementable for parameter optimization problems whose transfer functions are based on both continuous or discrete domain [40], [41]. Therefore, in this study, PI and repetitive control parameters of a three-phase boost PFC rectifier is optimized using a standard genetic algorithm (SGA).

Other than the optimization algorithm, the three-phase boost PFC rectifier performance is also influenced by the objective function. The most commonly used integral-based objective functions for PID controller parameters optimization are integrated absolute error (IAE), integrated squared error (ISE) and integrated time multiplied squared error (ITSE) [42]–[44]. Although these integral functions may reveal the control system optimization, the initial error would substantially affect the value of the ISE and IAE. Thus, it contributes to high-frequency resonance, poor steady-state characteristics and longer settling times (t_s). Meanwhile, ITSE can overcome the drawback of ISE criterion, but detailed and thorough analysis has shown that the $\%M_p$ percentage was high in studies using ITSE [45]–[48]. To address integral-based objective function issues, Zwe-Lee Gaing (ZLG) proposed a time-domain objective function based on the combination of dynamic performance indices M_p, t_r, t_s and E_{ss} [49]. However, ZLG objective function improves the efficiency of PI controller at the cost of high peak time (t_p) and t_s [49]–[51]. Furthermore, control parameters optimization using ZLG objective function is based on single weighting factor β and consequently provides one degree of freedom (DOF) for parameters optimization. Although, the ZLG objective function is one of the most widely used objective function, which shows significant performance for tuning PI controller for various systems [30], [50]–[55]. However, since the objective function is based on the combination of dynamic performance indices M_p, t_r, t_s, and Ess, it is effective for single control loop PI parameters optimization, primarily for the outer voltage loop. As the three-phase boost PFC rectifier contains multiple control loops, particularly after adopting the PI-repetitive controller for the inner current loop, the design parameters need to be further optimized. Hence, to overcome the ZLG objective function disadvantages for parameter optimization mainly because of the limited degree of freedom (DOF) in multiple control loops, this paper improves the ZLG objective function by two DOF. The proposed objective function introduces an additional weighting factor termed as emphasis factor γ.

This study performs inner current loop (PI-RC) parameters and outer voltage loop (PI) parameters optimization under a fixed loading condition using SGA, termed as SGA-PIR controller. Furthermore, in demonstrating how to employ the SGA-PIR controller to get the optimal controller parameters for a three-phase boost PFC rectifier. Two evaluation functions have also been proposed to examine whether the proposed method has better control performance in terms of THD reduction and improving dynamic performance indices.

Following the discussion above, the authors are encouraged to undertake the currently proposed research with the novelties mentioned below:

1) Previous work is primarily based on the parameter optimization of the PI controller only. However, this paper proposed parameter optimization of both PI and repetitive controller. Furthermore, for a three-phase boost PFC system, the existing ZLG objective function is modified by adding two degrees of freedom to optimize the PI and RC parameters effectively. Thus, improving controller performance in terms of THD reduction and dynamic performance indices.
2) ZLG and other objective functions such as IAE, ISE and ITSE have limitations since these functions are primarily adopted for the control parameters optimization for the single control loop only. However, by introducing two degrees of freedom, the proposed

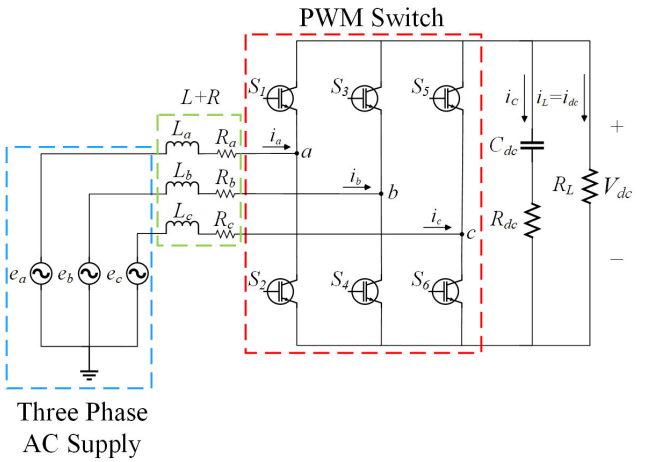

FIGURE 1. Topology for three-phase two-level boost PFC rectifier.

methodology has provided flexibility for control parameters optimization of multiple control loops.

3) Two evaluation functions have also been proposed to verify the effectiveness of the proposed SGA-PIR controller.
4) Simulations are intensively performed to validate new objective function, mainly for the second DOF emphasis factor γ. Besides, PI and RC optimized results are also compared with ISE, IAE, ITSE and ZLG objective functions using the SGA approach for a fair comparison. The comparative results demonstrate the superiority of the proposed objective function. The stability performance of the proposed SGA-PIR controller was methodically investigated using Nyquist and Bode plot analysis.
5) Finally, experimental test results for dynamic performance analysis (M_p, t_r, t_s and E_{ss}) and THD are also provided on a 5kW laboratory based three-phase boost PFC rectifier. The experimental tests are based on the best tuned controller parameters results and thus, the purpose is to validate the effectiveness of the proposed SGA-PIR controller. The results justified the feasibility of the proposed SGA-PIR controller tuning method.

II. THREE-PHASE TWO-LEVEL BOOST PFC RECTIFIER AND ITS MATHEMATICAL MODEL

The circuit topology of the three-phase two-level boost PFC rectifier is shown in Fig. 1. In this study, the proposed methodology is implemented on a three-phase PFC rectifier that mainly adopts the boost inductor and is a typical structure in the PFC topology. Therefore, the LCL-based filter used to suppress the switching ripples are common in grid-connected converters such as new energy generation or active power filter (APF) and hence not considered in this case.

To discuss the working principle of a three-phase boost PFC rectifier. The mathematical model of the system must be established [1], [2]. Then, the static *abc* coordinate system corresponding to the three-phase system is applied using Clark transformation. Similarly, the *dq* coordinate system obtained by Park transformation [56], [57] has greatly reduced the system control loop design complexity and improves the system response speed.

The three-phase boost PFC rectifier state-space equation in the three-phase stationary coordinate system [1], can be written as

$$\begin{cases} L\dfrac{di_a}{dt} = e_a - Ri_a - \dfrac{2S_a - S_b - S_c}{3}V_{dc} \\ L\dfrac{di_b}{dt} = e_b - Ri_b - \dfrac{2S_b - S_a - S_c}{3}V_{dc} \\ L\dfrac{di_c}{dt} = e_c - Ri_c - \dfrac{2S_c - S_a - S_b}{3}V_{dc} \\ C\dfrac{dV_{dc}}{dt} = S_a i_a + S_b i_b + S_c i_c - i_L \end{cases} \tag{1}$$

where e_a, e_b, and e_c are the three-phase input voltages i_a, i_b, and i_c represent the three-phase input currents. Similarly, $L_a = L_b = L_c = L$ represents the three-phase AC side filter inductor; and $R_a = R_b = R_c = R$ denotes the corresponding filter inductor parasitic resistances. V_{dc} is the output DC voltage and R_L is the load resistance. C_{dc} is the DC-link capacitor with parasitic resistance R_{dc} connected to the rectifier DC side, where $i_L = i_{dc} = V_{dc}/R_L$ denotes the load current. Correspondingly, $S_i(i = a, b, c)$ represents the bridge leg switching function, where $S_a = 1$ defines S_1 is on, and S_2 is off. Similarly, $S_a = 0$ defines S_1 is off, and S_2 is on.

By transforming (1) into a two-phase *dq* coordinate system [57], the (2) can be obtained as

$$\begin{cases} L\dfrac{di_d}{dt} = e_d - Ri_d + \omega Li_q - S_d V_{dc} \\ L\dfrac{di_q}{dt} = e_q - Ri_q - \omega Li_d - S_q V_{dc} \\ C\dfrac{dV_{dc}}{dt} = \dfrac{3}{2}(S_d i_d + S_q i_q) - i_L \end{cases} \tag{2}$$

where $\omega = 100\pi$ rad/s corresponds to the sinusoidal input voltage angular frequency, e_d, e_q denotes the active and reactive voltage components in the *dq* coordinate scheme, respectively. Similarly, i_d, i_q denote the active and reactive current components, and S_d, S_q represents the *dq* coordinate system switching functions, respectively.

A. INNER CURRENT LOOP PARALLEL PI-REPETITIVE (PIR) CONTROLLER DESIGN

The inner current loop aims to minimize the line-side current harmonics and keep close unity power factor with the PIR controller. PI controller with *dq* current reference is model initially. Then the parallel structure PI-repetitive controller is used to improve THD [19], [23]. Current loop Ldi_d/dt and Ldi_q/dt in (2) can be expressed as

$$\begin{cases} L\dfrac{di_d}{dt} = e_d - Ri_d + \omega Li_q - V_d \\ L\dfrac{di_q}{dt} = e_q - Ri_q - \omega Li_d - V_q \end{cases} \tag{3}$$

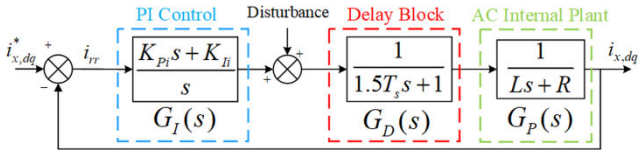

FIGURE 2. The equivalent block diagram of the inner current loop.

where $V_d = S_d V_{dc}$ and $V_q = S_q V_{dc}$ denote the manipulating variables of the d-axis (active) and q-axis (reactive) current.

From (3), it is clearly shown that the d-axis and q-axis current dynamics of the three-phase PFC rectifier are nonlinear and have strong coupling. Hence current regulator, after being adopted by the PI controller, the decoupled d-axis (active) and q-axis (reactive) current equations, i_d and i_q can be written as [34]

$$\begin{cases} i_d = \dfrac{(K_{Pi} + \frac{K_{Ii}}{s})(i_d{}^* - i_d)}{Ls + R} \\ i_q = \dfrac{(K_{Pi} + \frac{K_{Ii}}{s})(i_q{}^* - i_q)}{Ls + R} \end{cases} \tag{4}$$

where K_{Pi}, K_{Ii} is the inner current loop proportional and integral coefficient. Similarly, i_d and i_q respectively are the active and reactive current; $i_d{}^*$ and $i_q{}^*$ are the reference currents in dq coordinate system. The denominator term $Ls + R$ shows the AC internal plant model for the three-phase boost PFC rectifier inner current loop.

Based on (4), the inner current loop can be designed in the closed-loop form as shown in Fig. 2, where $i_{x,dq}$ is the output current and $i_x{}^*, dq$ is the reference current in dq reference frame. Similarly, $G_I(s)$ and $G_P(s)$ respectively represent the PI controller and AC internal plant model transfer function. As referred to [58], for real-time implementation in the digital controller such as DSP, a first-order delay block $G_D(s)$ is considered as illustrated in Fig. 2. Similarly, the same PI parameters for both dq current quantity is examined. Hence, $i_{x,dq}$ and $i_x{}^*, dq$ are referred to both d-axis (active) and q-axis (reactive) current quantity. In fact, to achieve close unity power factor, the reactive current i_q must be zero. Therefore, $i_q{}^* = 0$ and by the outer voltage loop controller, $i_d{}^*$ will be determined [34]. Hence, further analysis has been carried out by considering $i_{x,dq} = i_d$ and $i_x{}^*, dq = i_d{}^*$, thus making the investigation simpler and straightforward. Moreover, the considered assumption does not influence the dynamic response or stability of the system.

To improve the harmonics suppression capability of a three-phase boost PFC rectifier. Parallel structure PI-repetitive controller can be designed for the overall inner current loop as shown in Fig. 3, where $G_{RC}(z)$ is the repetitive controller, $G_{PD}(z)$ is the embedded transfer function for both internal plant model and delay transfer function. Similarly, $G_{IRC}(z)$ is the transfer function of parallel structure PI and repetitive controller, $i_{rr}(z)$ is the error current and is defined as $i_d{}^*(z) - i_d(z)$. Furthermore, the disturbance signal $i_{xk}(z)$ is transferred equivalently to the output side of $G_{PD}(z)$ for convenience.

TABLE 1. System parameters of three-phase boost PFC rectifier.

Symbol	Values	Description
$3\,\varphi$	381V	3 phase AC supply
L	4.5mH	Line inductor
R_L	98Ω	Load resistor
C_{dc}	1.5mF	DC link capacitor
R, R_{dc}	0.01Ω	L and C_{dc} parasitic resistors
V_{dc}	700V	DC link voltage
P	5kW	Rated active power
f_{sw}	16kHz	Switching/sampling frequency
f_L	50Hz	Fundamental/line frequency

From Fig. 3, we can infer that the relationship for the output current can be expressed as

$$i_d(z) = \frac{G_{PD}(z)G_{IRC}(z)}{1 + G_{PD}(z)G_{IRC}(z)} i_d^*(z) + \frac{1}{1 + G_{PD}(z)G_{IRC}(z)} i_{xk}(z) \tag{5}$$

where $i_{xk}(z)$ is the disturbance current and $i_d{}^*(z)$ is the d-axis reference current. According to (5), overall inner current closed-loop transfer function $G_{CLi}(z)$ from $i_d(z)$ and $i_d{}^*(z)$ can be expressed as

$$G_{CLi}(z) = \frac{i_d(z)}{i_d{}^*(z)} = \frac{G_{PD}(z)G_{IRC}(z)}{1 + G_{PD}(z)G_{IRC}(z)} \tag{6}$$

where

$$G_{IRC}(z) = G_I(z) + G_{RC}(z)$$

From Fig. 3, the transfer function of the repetitive controller $G_{RC}(z)$ is defined as

$$G_{RC}(z) = \frac{z^{-N} K_r z^m S(z)}{1 - Q(z) z^{-N}} \tag{7}$$

where $K_r z^m S(z)$ is a compensator used for amplitude and phase compensation. Among them, K_r is the repetitive controller gain, z^m is a leading element compensating the delay of phase, $S(z)$ is a low-pass filter used to filter out high-frequency interference components, respectively. Similarly, $Q(z)$ is a filter constant used to solve the object model inaccuracies and boost system robustness. N is the coefficient and is defines as f_{sw}/f_L. Thus, within one repetitive control cycle, there are $N = 320$ error samplings. Among five repetitive controller parameters, K_r, m, $S(z)$, $Q(z)$, N, two of them $S(z)$, N are mainly based on the system parameters, as mentioned in Table 1. Moreover, $Q(z)$, N can be easily calculated analytically. Whereas K_r, z^m, $Q(z)$ are difficult to find analytically and primarily based on a trial-and-error approach.

Hence, the parameter $S(s)$, which can calculate analytically, is simply a second-order low-pass filter and is defined as

$$S(s) = \frac{\omega_n^2}{s^2 + 2\xi\omega_n s + \omega_n^2} \tag{8}$$

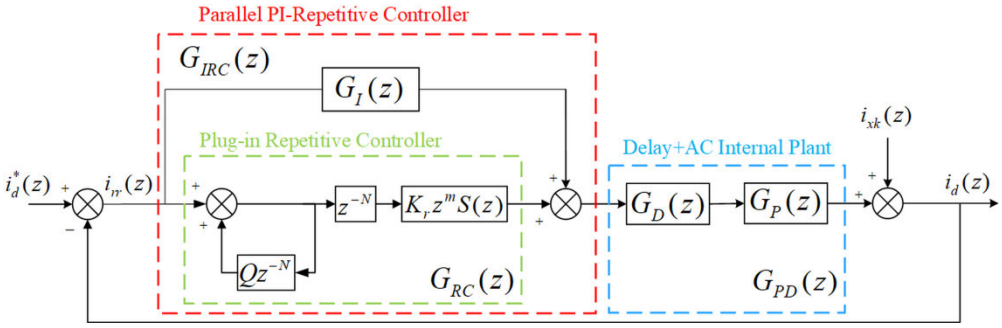

FIGURE 3. Implementation of parallel structure digital PI-repetitive controller for overall inner current loop of a three-phase PFC rectifier system.

where ω_n is the corner angular frequency, ξ is the damping ratio. The system will compensate harmonic currents within 50 times and since the fundamental frequency is $f_L = 50$ Hz; therefore, the corner frequency $f_n = 50 \times 50 = 2.5$ kHz, $\omega_n = 5000\pi\ rad/s$ with the damping ratio $\xi = 0.707$ is selected. Thus, the discretization of $S(z)$ with $f_{sw} = 16$ kHz can be written as

$$S(z) = \frac{0.1245z^2 + 0.249z + 0.1245}{z^2 - 0.7845 + 0.2826} \tag{9}$$

The characteristic polynomial of the overall inner current loop controller is defined using (6) as

$$1 + G_{PD}(z)G_{IRC}(z) = 0 \tag{10}$$

By substituting the value of $G_{RC}(z)$ from (7) into (10), the following equation can be obtained [21]

$$\begin{aligned}\Theta &= [1 - z^{-N}Q][1 + G_I(z)G_{PD}(z)] \\ &\quad + z^{-N}K_r z^m S(z)G_{PD}(z) = 0 \\ &= [1 + G_I(z)G_{PD}(z)]\left\{1 - z^{-N}[G_{PR}(z)]\right\} \\ &= \Theta_1\Theta_2 \end{aligned} \tag{11}$$

where

$$G_{PR}(z) = Q(z) - S(z)K_r z^m \frac{G_{PD}(z)}{1 + G_I(z)G_{PD}(z)}$$

In the following (12)-(13),Θ_1 and Θ_2, respectively, are the expressions for the PI controller alone, PI-repetitive controller and can be defined as

$$\Theta_1 = [1 + G_I(z)G_{PD}(z)] \tag{12}$$

$$\Theta_2 = 1 - z^{-N}\left[Q(z) - S(z)K_r z^m G_{PIi}(z)\right] \tag{13}$$

where $G_{PIi}(z)$ is an inner current closed-loop transfer function without a repetitive controller, expressed as

$$G_{PIi}(z) = \frac{G_{PD}(z)}{1 + G_I(z)G_{PD}(z)} \tag{14}$$

Equations (6), (12)-(14) have derived for two conditions: (1) when PI controller is used alone (2) with parallel structure PI-repetitive controller. These conditions are used for measuring THD, power factor, and stability analysis within the unit circle. Besides, (12)-(14) revealed that when parallel PI-repetitive control structure is adopted, the necessary and sufficient condition for the stability of the system constitutes that the poles of the closed-loop transfer function, i.e., roots of both terms Θ_1 and $\Theta_2$must be located inside the unit circle, defined using [19]

$$\left|z^{-N}Q(z) - z^{-N}S(z)K_r z^m G_{PIi}(z)\right| < 1 \tag{15}$$

The roots $1 + G_I(s)G_{PD}(s) = 0$ requirement can be fulfilled by adequately selecting the $G_{PIi}(z)$ controller transfer function and thereby ensuring that the condition $\left|z^{-N}Q(z) - z^{-N}K_r z^m S(z)G_{PIi}(z)\right| < 1$ is met for the stability. Then, by realizing $z = e^{j\omega}$, the condition can be simplified using small gain theorem [18] and can be expressed as

$$\begin{aligned}&\left|Q(e^{j\omega t}) - K_r e^{jm\omega t}S(e^{j\omega t})G_{PIi}(e^{j\omega t})\right| < 1 \\ &\omega \in [0, \pi/T_s]\end{aligned} \tag{16}$$

Define $H(e^{j\omega t}) = Q(e^{j\omega t}) - K_r e^{jm\omega t}S(e^{j\omega t})G_{PIi}(e^{j\omega t})$ such that the end of the vector $H(e^{j\omega t})$ should never exceed the unit circle.

B. VOLTAGE LOOP PI CONTROLLER DESIGN

The outer voltage loop PI controller has been used to ensure the DC link voltage dynamic stability due to line voltage fluctuation or step load variation.

From (2), the outer voltage loop equation can be expressed as

$$C\frac{dV_{dc}}{dt} = \frac{3}{2}(S_d i_d + S_q i_q) - i_L \tag{17}$$

The PI form of the outer DC voltage controller can be written as follows

$$C\frac{dV_{dc}}{dt} = K_{Pv}(V_{dc}{}^* - V_{dc}) + \frac{K_{Iv}}{s}(V_{dc}{}^* - V_{dc}) \tag{18}$$

where K_{Pv} and K_{Iv} is the proportional and integral coefficient of the outer voltage loop PI controller. V_{dc} is the output DC voltage and $V_{dc}{}^*$ is the reference output DC voltage.

The control block diagram of the outer voltage loop using PI controller is shown in Fig. 4. Suppose, i_σ is the amplitude of the input three-phase current, where 'σ' is the modulation degree of the PWM wave. Then the current i_d is assumed to

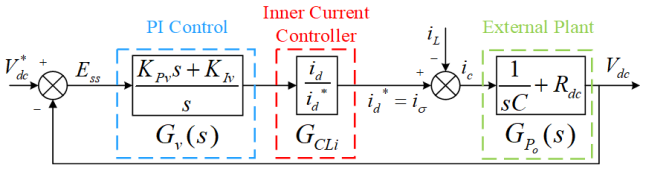

FIGURE 4. The equivalent block diagram of the outer voltage loop.

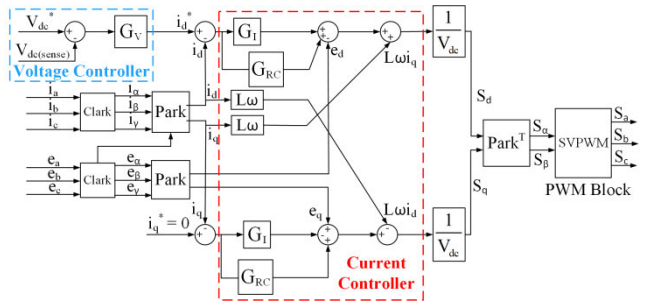

FIGURE 5. Complete control structure of three-phase PFC rectifier system with inner current control loop and *dq* axes decoupler.

follow the given reference current value $i_d{}^*$ entirely with the output of the outer loop controller having the magnitude of the input current i_σ. Hence, $i_d{}^*$ is taken as the given value of the inner current loop, thus realizing the double closed-loop control of voltage and current for a three-phase PFC rectifier.

According to Fig. 4, by neglecting load current i_L, the overall voltage closed-loop transfer function in discrete domain representation $G_{CLv}(z)$ can be expressed as

$$G_{CL_v}(z) = \frac{V_{dc}(z)}{V_{dc}{}^*(z)} = \frac{G_v(z)G_{CLi}(z)G_{P_o}(z)}{1 + G_v(z)G_{CLi}(z)G_{P_o}(z)} \tag{19}$$

where $G_{CLi}(z)$, $G_{Po}(z)$, respectively, in the discrete domain represents the inner current closed-loop transfer function and the external plant model transfer function with parasitic resistance R_{dc}. Similarly, $G_v(z)$ is the PI controller transfer function for the outer voltage loop. Correspondingly, from Fig. 4, the discrete transfer function from $E_{ss}(z)$ to $V_{dc}^*(z)$ can be derived as

$$E_{ss}(z) = V_{dc}^*(z) - V_{dc}(z) = \frac{V_{dc}^*(z)}{1 + G_v(z)G_{CLi}(z)G_{P_o}(z)} \tag{20}$$

where $E_{ss}(z)$ is the error function in the discrete domain. The overall control structure of the three-phase boost PFC rectifier is shown in Fig. 5.

In the aforementioned analysis, the bilinear transformation has been used to convert the transfer function of the PI controller for both inner current and outer voltage control loops from continuous domain to discrete domain formulated as

$$G_{PI}(z) = K_P + \frac{K_I}{s} = K_P + K_I / \frac{2}{T_s}\frac{1 - z^{-1}}{1 - z^{-1}} \tag{21}$$

The conventional method of parameter tuning is based on many assumptions and simplifications; the inner current and outer voltage loop control parameters need to be designed separately. Then, the PI and repetitive controller parameters must be changed in a wide range according to the designer's expertise. In general, obtaining the system controller parameter values using the traditional method [24] make the optimum result difficult and time-consuming. Since it requires numerical procedure and simulation process with a trial-and-error approach. Therefore, this study proposed a new objective function to speed up the tuning process of PI-repetitive controller parameters of a three-phase boost PFC rectifier using SGA-PIR controller, described in the following section.

III. PROPOSED OBJECTIVE FUNCTION FOR PI AND RC CONTROLLER PARAMETERS OPTIMIZATION

A. MATHEMATICAL FORMULATION OF THE PROPOSED OBJECTIVE FUNCTION

The three-phase boost PFC rectifier performance is evaluated based on the dynamic performance indices (M_p, t_r, t_s and E_{ss}), minimum THD and close unity PF. Three commonly used integral-based objective functions applied in a control parameter optimization are ISE, IAE and ITSE [42]–[44]. These integral-based objective functions are defined as follows [43]

$$ISE = \int_0^{t_{sim}} e^2(t)dt \tag{22}$$

$$IAE = \int_0^{t_{sim}} |e(t)|dt \tag{23}$$

$$ITSE = \int_0^{t_{sim}} te^2(t)dt \tag{24}$$

where t_{sim} is the simulation duration and $e(t) = y^*(t) - y(t)$ is the error signal.

Meanwhile, in literature [30], [50]–[55], widely adopted time-domain objective function has been proposed by Zwe-Lee Gaing (ZLG) and is defined as [49]

$$ZLG = (1 - e^{-\beta}).(M_p + E_{ss}) + e^{-\beta}(t_s - t_r) \tag{25}$$

where β is a weighting factor whose ranges vary from 0.5 to 1.5. From (25), it is observed that ZLG objective function is primarily based on the dynamic performance indices (M_p, t_r, t_s and E_{ss}), which can mainly adequate for the parameter optimization of a single voltage loop PI controller. However, a system such as the three-phase PFC rectifier contains two control loops, i.e., inner current and outer voltage loop. Therefore, the ZLG objective function does not provide flexibility due to limited DOF for parameters optimization of multiple control loops. In addition, research has shown that the optimization of parameters using the ZLG objective function, t_s and t_p were high [49]–[51]. Hence, to overcome the disadvantage of the ZLG objective function, a new performance criterion based on the ZLG objective function is proposed in this paper and is defined as follows:

$$\min{}_{\theta:\,stabilizing}\ R(\theta) = \left[\alpha(M_p + E_{ss}) + (1 - \alpha)(t_s - t_r)\right]^\gamma \tag{26}$$

where θ is [K_r, m, $Q(z)$, K_{Pi}, K_{Ii}, K_{Pv}, K_{Iv}], α is the weighting factor and γ is the emphasis factor with ranges $\alpha, \gamma \in [0.1, 0.9]$. Similarly, M_p, E_{ss} respectively represents the overshoot and steady-state error, t_r, t_s, respectively, characterizes the rise time and settling time. Moreover, t_r is the time needed to increase the response from 10% - 90% and t_s is the time expected to settle within 5% of the output parameter [59]. The value of α can set to greater than 0.5 to minimize steady-state error and overshot. Conversely, decreasing the value of α from 0.5 will reduce the t_r and t_s. Similarly, γ is the emphasis factor influences the weighting factor α for the controller parameters optimization of multiple control loops and will define the solution space. In fact, the multiplying weighting factor α ranging [0.1, 0.9] in (26) is based on the same conversion factor $1 - e^{-\beta}$ with $\beta \in [0.8, 1.5]$ used in (25) and hence will not influence the dynamic performance indices multiplying factor $(M_p + E_{ss})$, $(t_s - t_r)$ respectively. Therefore, it is noteworthy that the modified ZLG objective defined in (26) is presented in a more simplified form with two DOF. Consequently, it can provide more flexibility for controller parameters optimization.

Although using (26) may cause ambiguity with the inner current loop parameters since the objective function mainly reflects the outer voltage control loop dynamic characteristics M_p, t_r, t_s and E_{ss}. However, suppose two separate objective functions are considered for both inner current and outer voltage loop. In that case, the design complexity will increase many folds, especially giving different weights to different objective functions. Therefore, it is more convenient and straightforward to use a single objective function with two DOF for both control loops. Moreover, the analysis is justifiable since E_{ss} used in (26) is based on (20), which contains the error transfer function including the inner current loop controller parameters. Besides, it's a hybrid approach; once the controller parameter values are found using the proposed objective function, the results are subsequently analyzed using simulation for PF, THD and dynamic performance indices. Hence, if the simulation result is not satisfactory, then (26) is penalized with a higher degree of emphasis factor γ and check the system performance.

Therefore, by properly using the value of weighing factor α and emphasis factor γ, the performance criterion $R(\theta)$ can satisfy the designer requirements. In this paper, a higher priority is considered for $M_p + E_{ss}$. In fact, the controller performance characteristics such as steady-state error (E_{ss}) and overshot (M_p) are more critical and sensitive for any system disturbance or grid fluctuation and may damage the system. Therefore, in this study, the weighting factor $\alpha = 0.7$ is set. Furthermore, the weighting factor value around 0.7 for $(M_p + E_{ss})$ has also been found optimum in [30], [49]. Hence, the analysis has only been performed for the emphasis factor $\gamma \in [0.1, 0.9]$. However, the value of weighting factor α can be varied depending upon the designer's requirement and satisfaction.

TABLE 2. Max and min ranges for SGA-PIR controller.

Symbol	Description	Ranges [min, max]
K_{Ii}	Current loop integral gain	[1, 20]
K_{Pi}	Current loop proportional gain	[1, 10]
$Q(z)$	Filter coefficient	[0.90, 0.99]
K_r	Repetitive controller gain	[0, 2]
m	Delay link	[2, 8]
K_{Iv}	Voltage loop integral gain	[1, 5]
K_{Pv}	Voltage loop proportional gain	[0.1, 0.5]

B. CONSTRAINTS OF THE PROPOSED OBJECTIVE FUNCTION

It is essential to optimize the control system parameters by adequately setting the lower and upper limits of PIR controller gains. The boundaries to be used in the problem of optimization are therefore defined as follows

$$K_{Pi}, K_{Ii}, K_{Pv}, K_{Iv}, m, Q, K_r \propto (min, max) \tag{27}$$

where *min* and *max*, respectively, represent the minimum and maximum gain values of the PIR controller.

In this study, to find the optimal PIR controller gains and make an effective comparison with other objective functions, *min* and *max* ranges of the controller gains are defined in Table 2. Indeed, the parameters [K_r, m, $Q(z)$] ranges for the repetitive controller have been set according to the investigator's analysis and recommendations [19]–[23]. Such as, K_r is a repetitive controller gain and its larger value ensures fast system response, but if it is too large, it will make the system unstable. Therefore, K_r $(0 < K_r \leq 2)$ has been set. Similarly, z^m is the phase compensator used to compensate for the phase delay of the control system in the low-frequency region and thus, $m(2 < m \leq 8)$ is sufficient. Likewise, $Q(z)$ enhances the robustness by slightly attenuating the integration action, which can be a constant and set between $(0.9 < Q(z) \leq 0.99)$. Conversely, using the Ziegler-Nichols method [26], PI gain values are generated as a starting point.

IV. EVALUATION FUNCTION FOR THE DOUBLE CLOSED-LOOP PIR CONTROLLER

A three-phase PFC rectifier is composed of two control loops. Therefore, two evaluation functions are proposed to evaluate the optimized PI and RC parameter values in terms of THD reduction and dynamic performance indices improvement.

The inner current loop with a parallel structure PI-repetitive controller aims to provide a close unity power factor with the total harmonic's distortion of less than 5% [60]. Therefore, the evaluation function J_i has been mainly designed for evaluating THD results. The evaluation function for the inner current loop J_i can be defined as

$$J_i = \frac{l_f}{T_f \sum_{k=0}^{l_f} e_{THD_k}} \tag{28}$$

where $e_{THD} = THD_{ref} - THD_{sim}$ is the THD error, T_f is the total test frequency for measuring THD, and l_f is the length

of test frequency interval. In this analysis, $T_f = 1000$ Hz and $l_f = 2.5$ Hz are considered. The reference value for THD_{ref} is set as 5%, whereas THD_{sim} is the simulated value of THD. Moreover, the optimized controller parameter values are verified using fast Fourier transform (FFT) analysis to measure the THD and thus, the negative value of J_i shows that THD $> 5\%$.

Similarly, to calculate the maximum value of the evaluation function, (28) can be defined as

$$J_i' = \frac{1}{J_i} \tag{29}$$

Meanwhile, the evaluation function for the outer voltage loop can be defined as the reciprocal of objective function $R(\theta)$, written as

$$J_v = \frac{1}{R(\theta)} \tag{30}$$

where $R(\theta)$ is defined in (26), which characterizes the overall SGA-PIR controller performance criteria. The evaluation functions J_i' and J_v are described in the reciprocal form, which implies that the smaller the value of J_i and $R(\theta)$, the higher its evaluation value.

The approaches mentioned above (sections III-IV) can reduce the complexity of the multi-optimization problem in a way that instead of using multiple objective functions for optimizing controller parameters. A single objective function (26) and two evaluation functions (28), (30) can effectively optimize and estimate the performance of PIR controller parameters.

V. IMPLEMENTATION OF PIR CONTROLLER USING SGA

A. SGA IMPLEMENTATION

In this paper, to improve the THD and dynamic response characteristics (M_p, t_r, t_s and E_{ss}) of a three-phase boost PFC rectifier, the proposed objective function $R(\theta)$ is implemented using a standard genetic algorithm (SGA), also called SGA-PIR controller. As one of the heuristic algorithms, GA is a search and selection algorithm based on the principle of natural evolution and population genetics [38]. It consists of three parts: encode and decode, assessment of fitness and iteration of evolution. In addition, replication, crossover, mutation and even inversion are included in the evolution iteration [39].

A population of individuals such as x_i $(i = 1, \ldots, n)$, where n denotes the population size, is maintained by SGA. Each individual is a possible solution to the problem. Furthermore, to provide a measure of fitness, individuals are tested. Then, the fitter individual's selection produces a new population iteration $n+1$ (selection step). Moreover, because of crossover and mutation operators to create new solutions, certain individuals in the new population are undergoing the phase of evolution. The search converges after several generations and, if efficient, the best solution for an individual is the optimal solution.

In this case, there are seven unoptimized controller parameters in θ; therefore, SGA will find the best solution for each parameter in a solution space and as there are n individuals in a population. Hence the population dimension is $n \times 7$. All the biological terms or operators in SGA, such as selection, crossover and mutation will be implemented in the mathematical form, as shown in Fig. 6.

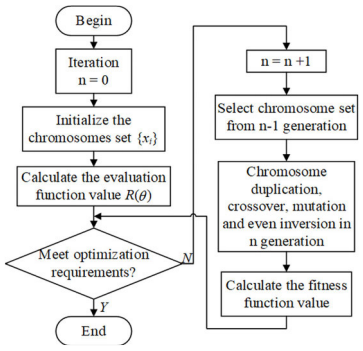

FIGURE 6. Flowchart of SGA implementation.

B. IMPLEMENTATION OF THE PROPOSED SGA-PIR CONTROLLER WITH SIMULATION PROCEDURE

The proposed SGA-PIR controller is used to determine the five optimal parameters [K_r, m, $Q(z)$, K_{Pi}, K_{Ii}] for the inner current loop. Similarly, two optimal parameters [K_{Pv}, K_{Iv}] for the outer voltage loop, so that a good step response output could be obtained from the controlled system.

The step-by-step procedure for implementing and validating the SGA-PIR controller is given below.

Step 1: Set the minimum and maximum ranges for the controller parameters [K_r, m, $Q(z)$, K_{Pi}, K_{Ii}, K_{Pv}, K_{Iv}] according to Table 2, as specified in section III-B. SGA-PIR controller will provide optimal parameter values by considering these ranges.

Step 2: According to the analysis discussed in section III-A, set the value of weighting factor $\alpha = 0.7$ in (26). Similarly, instead of changing the number of iterations and other SGA settings, only the emphasis factor γ varies from 0.1 to 0.9. SGA is used with various parameter settings, as listed in Table 3.

Step 3: Once the PIR controller parameters value are obtained, employ the Nyquist graphical technique for the inner current loop controller parameters to test the open-loop stability within the unit circle $H(e^{jwt}) < 1$ mentioned in (16). Furthermore, (6) and (14) have been used to test the closed-loop stability using a bode plot for PI-RC and PI control alone, respectively. The sufficient gain margin (GM) and phase margin (PM) to ensure the stability of the system are, respectively, 5dB to 10dB and 45^0 to 60^0 [61]. Therefore, the same stability margin has been followed in this analysis, especially the PM of 45^0 is sufficient as the digital controller is employed to test the hardware.

Step 4: To verify the outer voltage loop PI parameters [K_{Pv}, K_{Iv}], (19) has been employed to test the double closed-loop stability with the same stability margins mentioned in step 3. Furthermore, the necessary and sufficient condition for

TABLE 3. Parameter settings in SGA optimization.

Parameter	Value	Type
Population size	200	Randomly initiated
Fitness scaling	-	Proportional
Crossover	0.85	Intermediate
Mutation	-	Adaptive feasible
Selection	2	Tournament
Stopping criteria	50	Number of generations

the overall three-phase PFC rectifier stability is that the bandwidth (BW) of the inner current loop must be higher than the outer voltage loop [23]. Using the MATLAB step response simulation, calculate four dynamic performance criteria in the time domain, namely M_p, E_{ss}, $t_{r,}$ and t_s.

Step 5: In the proposed analysis, the objective function (26) and two evaluation functions (28), (30) are used to estimate the controller performance. Thus, once the SGA searches the PIR controller parameters, then J_i' and J_v are used to test the PIR controller gain values analytically to calculate the maximum value of evaluation functions. Simulation tool such as MATLAB FFT analyzer is used to measure THD.

Step 6: The objective function $R(\theta)$ is penalized with a higher degree of emphasis factor γ if any of the criteria mentioned in steps 3–5 is not fulfilled. However, there can be an exception and flexibility in these criteria based on the designer's experience and requirements.

VI. SIMULATION RESULTS AND DISCUSSION

The three-phase boost PFC rectifier control structure is tested to verify the proposed objective function $R(\theta)$. The simulations were performed using the MATLAB/Simulink model (Version R2018b) and GA toolbox on an intel i7, 4 GHz processor with 8GB RAM computer. In order to verify the second DOF emphasis factor (γ) feasibility, nine simulation examples with $\alpha = 0.7$ and $\gamma \in [0.1, 0.9]$ were performed for PIR controller parameters optimization. The PI and RC parameters optimized values for the three-phase boost PFC rectifier are summarized in Table 4, including comparative simulation results with existing objective functions, namely ISE, IAE, ITSE and ZLG. The simulations have been performed based on the system parameters mentioned in Table 1.

In the subsequent subsections, the essential findings of this analysis are demonstrated.

A. PERFORMANCE EVALUATION FOR INNER CURRENT LOOP

To determine the three-phase boost PFC rectifier stability performance. Nyquist and Bode plot analysis are performed based on PIR controller parameter values, as mentioned in Table 4. Thus, for the inner current loop PI-repetitive controller parameter results, the Nyquist plot is drawn to check the stability condition $H(e^{j\omega t})$, as shown in Fig. 7. The result shows that $H(e^{j\omega t})$ trajectories are inside the unit circle evaluated with different emphasis factors γ. Furthermore, as shown

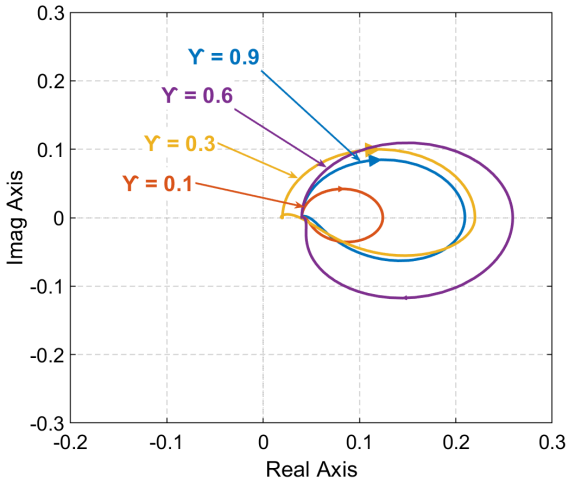

FIGURE 7. Nyquist plot $H(e^{j\omega t})$ using different values of $\gamma = [0.1, 0.3, 0.6, 0.9]$.

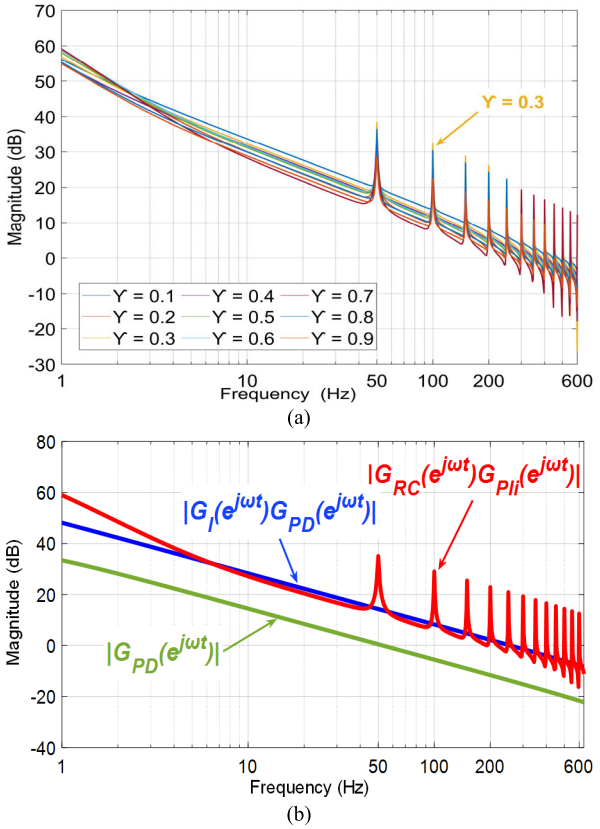

FIGURE 8. Open loop magnitude curves (a) with emphasis factor $\gamma \in [0.1, 0.9]$ (b) comparison with gains $|G_{PD}(e^{j\omega t})|$, $|G_I(e^{j\omega t})G_{PD}(e^{j\omega t})|$ and $|G_{RC}(e^{j\omega t})G_{PIi}(e^{j\omega t})|$ using $\gamma = 0.3$.

in the summarized results in Table 4, the best-optimized result in terms of lowest %THD has to be found at $\gamma = 0.3$. From the comparative results, it is revealed that among three integral-based objective functions, only ITSE has THD value less than 5% compared to ISE and IAE objective functions. Because the convergence speed in time and reached global minimum values for ITSE is better than ISE, IAE objective

TABLE 4. Summarized simulation results for SGA-PIR controller parameters.

Simulation Examples	γ	Inner current loop PI-repetitive controller parameters					Outer voltage loop PI parameters		MATLAB Simulation Result		$J_i^{'}$
		K_{Pi}	K_{Ii}	K_r	Q	m	K_{Pv}	K_{Iv}	%THD	PF	
Example 1	0.1	6.5	15.9	0.66	0.97	5	0.26	4.24	4.80	0.99	0.80
Example 2	0.2	9.0	18.9	1.70	0.98	8	0.26	4.56	2.10	0.99	11.6
Example 3	0.3	7.7	16.1	1.54	0.98	7	0.23	4.88	1.82	0.99	12.7
Example 4	0.4	9.3	19.7	1.60	0.98	4	0.30	4.32	3.23	0.99	7.08
Example 5	0.5	8.7	15.8	0.94	0.98	5	0.23	4.96	2.90	0.99	8.40
Example 6	0.6	9.7	18.2	1.10	0.98	6	0.30	4.00	2.38	0.99	10.4
Example 7	0.7	9.3	15.2	1.30	0.98	5	0.29	4.16	2.50	0.99	10.0
Example 8	0.8	8.0	19.3	1.47	0.98	6	0.30	4.48	2.17	0.99	11.3
Example 9	0.9	9.2	19.5	1.16	0.98	4	0.29	5.00	3.61	0.99	5.56
Comparative analysis with other objective functions											
SGA-ISE		5.1	18.0	0.20	0.99	4	0.29	4.32	7.45	0.99	-13.8
SGA-IAE		7.4	15.1	0.84	0.98	2	0.26	4.56	5.51	0.99	-2.04
SGA-ITSE		8.9	17.5	0.80	0.99	5	0.22	4.80	4.03	0.99	2.42
SGA-ZLG		8.7	15.8	1.24	0.98	3	0.30	4.08	4.47	0.99	2.12

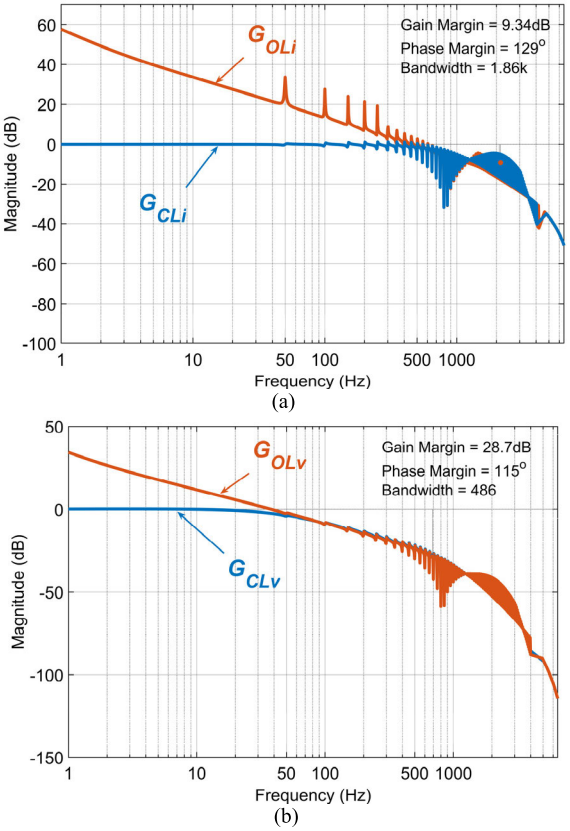

FIGURE 9. Open and closed-loop bode diagram (a) inner current loop (b) outer voltage loop.

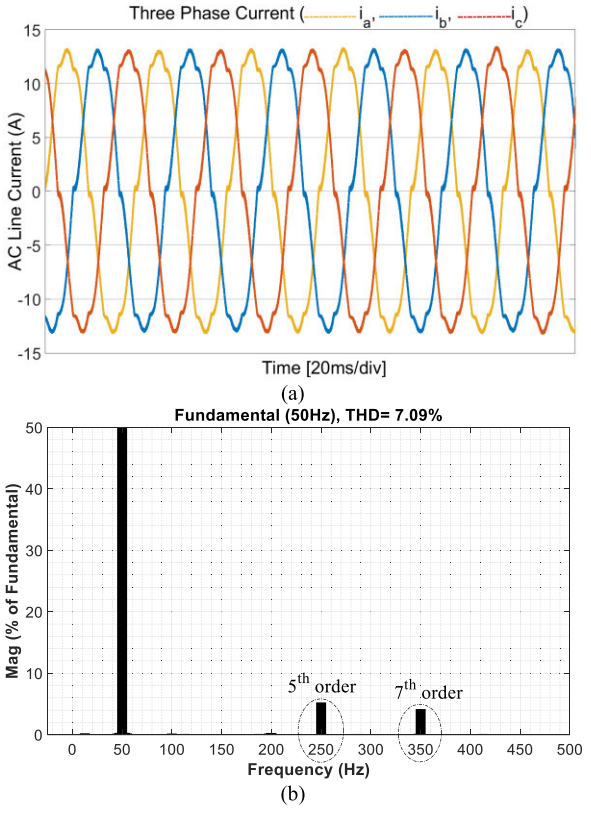

FIGURE 10. Three-phase PFC rectifier simulation results with PI controller (a) Three-phase line current (b) THD Analysis.

functions. On the other hand, although ZLG shows some performance with THD $< 5\%$; however, compared with the proposed objective function $R(\theta)$, the THD value has been much reduced using $\gamma = 0.3$. Hence, the results clearly demonstrate the effectiveness and superiority of the proposed objective function $R(\theta)$ after adopting the second DOF γ. Close unity power factor has also been achieved in all cases.

Fig. 8(a) shows the open-loop gain for the inner current loop with $\gamma \in [0.1, 0.9]$ values. Similarly, Fig. 8(b) shows the open-loop magnitude plot at $\gamma = 0.3$ for respectively, PIR controller $G_{RC}(e^{j\omega t})G_{PIi}(e^{j\omega t})$, PI controller with plant model $G_I(e^{j\omega t})G_{PD}(e^{j\omega t})$, and the plant model $G_{PD}(e^{j\omega t})$ only. The simulation results indicate that the PI-repetitive controller has the highest gain at the fundamental frequency, thus improving harmonic suppression capability compared with PI control alone.

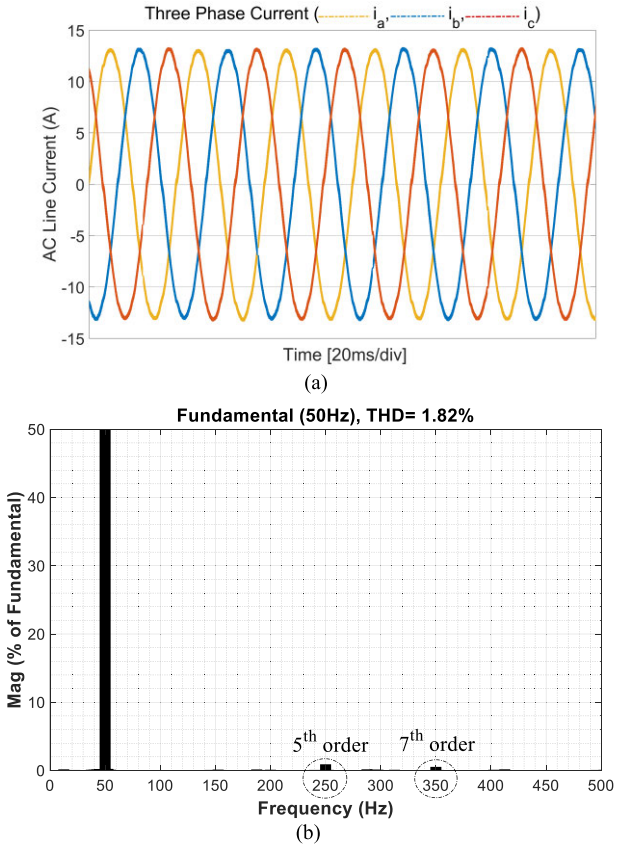

FIGURE 11. Three-phase PFC rectifier simulation results with parallel structure PI-repetitive controller (a) Three-phase line current (b) THD analysis.

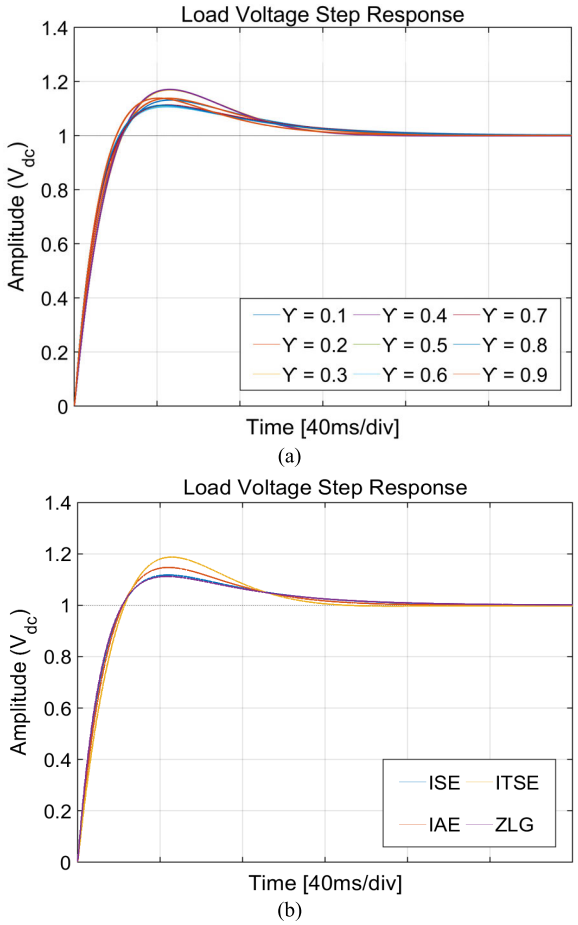

FIGURE 12. Step load voltage response simulation results for dynamic performance indices based on table 5 parameters (a) proposed SGA-PIR controller (b) other objective functions using SGA.

Fig. 9(a) and (b) show the open-loop (G_{OLi}, G_{OLv}) and closed-loop (G_{CLi}, G_{CLv}) magnitude bode diagram for the inner current and outer voltage loop based on PI-RC parameter values at $\gamma = 0.3$. Fig. 9 shows that GM and PM are higher than 5dB and 60^0, respectively. Hence, it fulfilled the necessary and sufficient conditions for the system's stability mentioned in steps 3, section V-B.

Fig. 10 and Fig. 11, show the simulation results of three-phase current waveforms and THD results using PI controller and PI-repetitive controller, respectively. The result shows that the THD value of the three-phase PFC rectifier with PI controller alone is 7.09%, which is higher than the desired THD $< 5\%$. Conversely, when SGA-PIR controller using emphasis factor $\gamma = 0.3$ is adopted, THD value is reduced to 1.82%. Hence, the results revealed that by using the proposed objective function $R(\theta)$, the inner current PI-repetitive control parameters optimization had better performance and reduced analytical processes, especially for the repetitive controller. Figures 10b and 11b also shown the dominance of 5^{th} and 7^{th} order harmonics.

B. PERFORMANCE EVALUATION FOR THE OUTER VOLTAGE LOOP

The purpose of the outer voltage PI control loop is to ensure the system dynamic stability in case of any step load variation. The main dynamic performance indices used in this paper for the evaluation purpose are M_p, t_r, t_s and E_{ss}. Hence, using (19), MATLAB simulations have been performed with step load function based on the PI controller's optimized values for the outer voltage loop, summarized in Table 4. Fig. 12(a) shows the step load voltage response of the three-phase boost PFC rectifier from no load to full load i.e., $R_L = 98\Omega$. Moreover, Fig. 12(b) shows the comparative step load response results with ISE, IAE, ITSE and ZLG objective functions controller parameters values as mentioned in Table 4.

Table 5 summarizes the dynamic performance for the three-phase boost PFC rectifier. Table 5 shows that at $\gamma = 0.6$, J_v has the highest evaluation value, mainly because of the minimum overshoot. However, from the analysis mentioned above, the minimum %THD is achieved using $\gamma = 0.3$. Thus, it is observed that at different values of emphasis factor γ. There is a trade-off between %THD and dynamic performance indices such as maximum overshoot M_p. Even though $\%M_p$ using $\gamma = 0.3$ is higher than emphasis factors $\gamma = 0.6$. However, the overshoot value is still 110.8V compared with 74.2V for $\gamma = 0.6$, which is acceptable and safe considering a PWM switch voltage rating of 1200V.

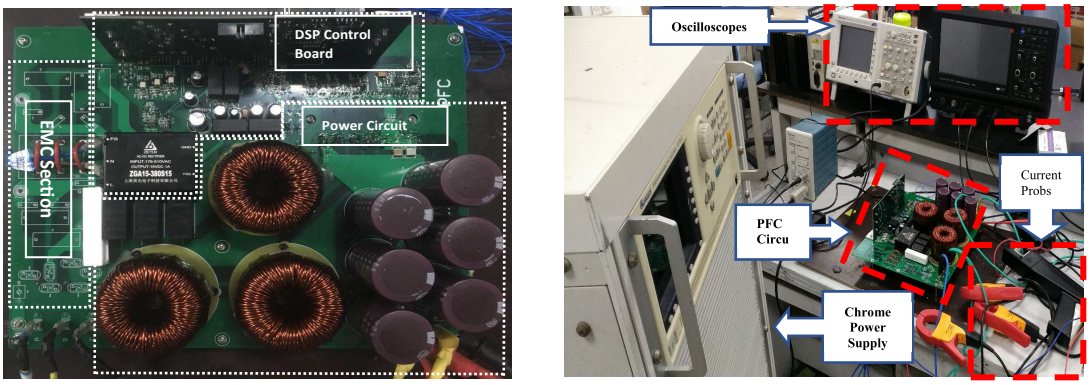

(a) (b)

FIGURE 13. Hardware module (a) PFC rectifier with DSP controller board (b) Experimental setup for testing hardware.

TABLE 5. Dynamic performance indices for double closed PIR controller.

Simulation Example	γ	Dynamic Performance Indices				J_v
		M_p (%)	E_{ss}	t_s (ms)	t_r (ms)	
Example 1	0.1	13.12	0	129.0	16.1	0.108
Example 2	0.2	13.78	0	123.2	16.4	0.103
Example 3	0.3	15.87	0	113.6	17.0	0.089
Example 4	0.4	16.04	0	112.4	17.4	0.088
Example 5	0.5	11.90	0	131.6	15.6	0.119
Example 6	0.6	10.61	0	134.4	15.4	0.126
Example 7	0.7	12.29	0	132.2	15.9	0.115
Example 8	0.8	12.11	0	128.8	15.5	0.117
Example 9	0.9	14.81	0	110.4	16.9	0.096
Comparative analysis with other objective functions						
SGA-ISE		13.23	0	123.4	16.3	0.107
SGA-IAE		14.69	0	115.8	16.9	0.097
SGA-ITSE		18.71	0	111.6	18.1	0.076
SGA-ZLG		12.20	0	128.6	15.8	0.116

Table 5 also shows the comparative analysis of the proposed objective function with other objective functions for dynamic performance indices. The results revealed that SGA-ITSE has the highest M_p compared with proposed and other objective functions. Correspondingly, t_s value using the ZLG objective function is higher. Hence, the results also justified the drawback of the ITSE and ZLG objective functions described in the previous sections. Summarized results in Table 5 also indicate that dynamic performance indices M_p, t_s and t_r are sensitive for the PI control gain (K_{Pv}, K_{Iv}) variation used for the outer DC voltage regulation. Since a small change in PI gain values, as mentioned in Table 4, can cause a significant change in controller performance. Therefore, parameter ranges such as mentioned in Table 2 are critical to ensure the proposed SGA-PIR controller stability and better performance. Furthermore, to evaluate the dynamic performance indices with other objective functions, the same evaluation function (30) is used without emphasis γ. The assumption is also justifiable since the SGA method is also used for comparative analysis.

Table 6 summarizes the percentage improvement in dynamic performance indices (M_p, t_r, t_s, E_{ss}) and THD using

TABLE 6. Percentage improvements using proposed SGA-PIR controller compared with other objective functions.

Objective functions	% Improvements based on proposed SGA-PIR controller				
	M_p (%)	E_{ss}	t_s (ms)	t_r (ms)	THD
	Evaluated at emphasis factor $\gamma = 0.6$				at $\gamma = 0.3$
SGA-ISE	19.80	0	-8.94	5.52	75.57
SGA-IAE	27.77	0	-16.01	8.87	66.96
SGA-ITSE	43.29	0	-20.43	14.91	54.83
SGA-ZLG	13.03	0	-4.51	2.53	59.28

$\gamma = 0.6$ and 0.3, respectively, for the proposed objective function with other objective functions. The negative sign shows at $\gamma = 0.6$; only t_s value is higher than other objective functions. Hence, the proposed controller proved better control performance in terms of THD, M_p and t_r at the cost of increased settling time t_s. It is also noteworthy that t_s is higher with $\gamma = 0.6$, though minimum t_s is achieved at $\gamma = 0.9$. Hence, it is observed that different values of γ can provide flexibility and be selected based on system designer requirements and priority-based approaches.

VII. EXPERIMENTAL RESULTS

Three-phase boost PFC rectifier experiments were performed using the system parameters mentioned in Table 1. Fig. 13(a) demonstrates the three-boost PFC rectifier prototype hardware with an embedded DSP controller board implemented with a TMS320F28335 DSP from Texas Instruments. Fig. 13(b) shows the experimental setup layout, including a chrome AC programmable source to protect the hardware and equipment.

A. STEADY-STATE PERFORMANCE FOR THD ANALYSIS

Figure 14 (a) shows the three-phase currents i_a, i_b, i_c waveforms of the three-phase boost PFC rectifier with PI controller alone. Fig. 14(c) shows FFT analysis of the line current i_a for THD evaluation. In this case, the experimental results are carried out based on PI parameters $K_{Pi} = 9.3$, $K_{Ii} =$

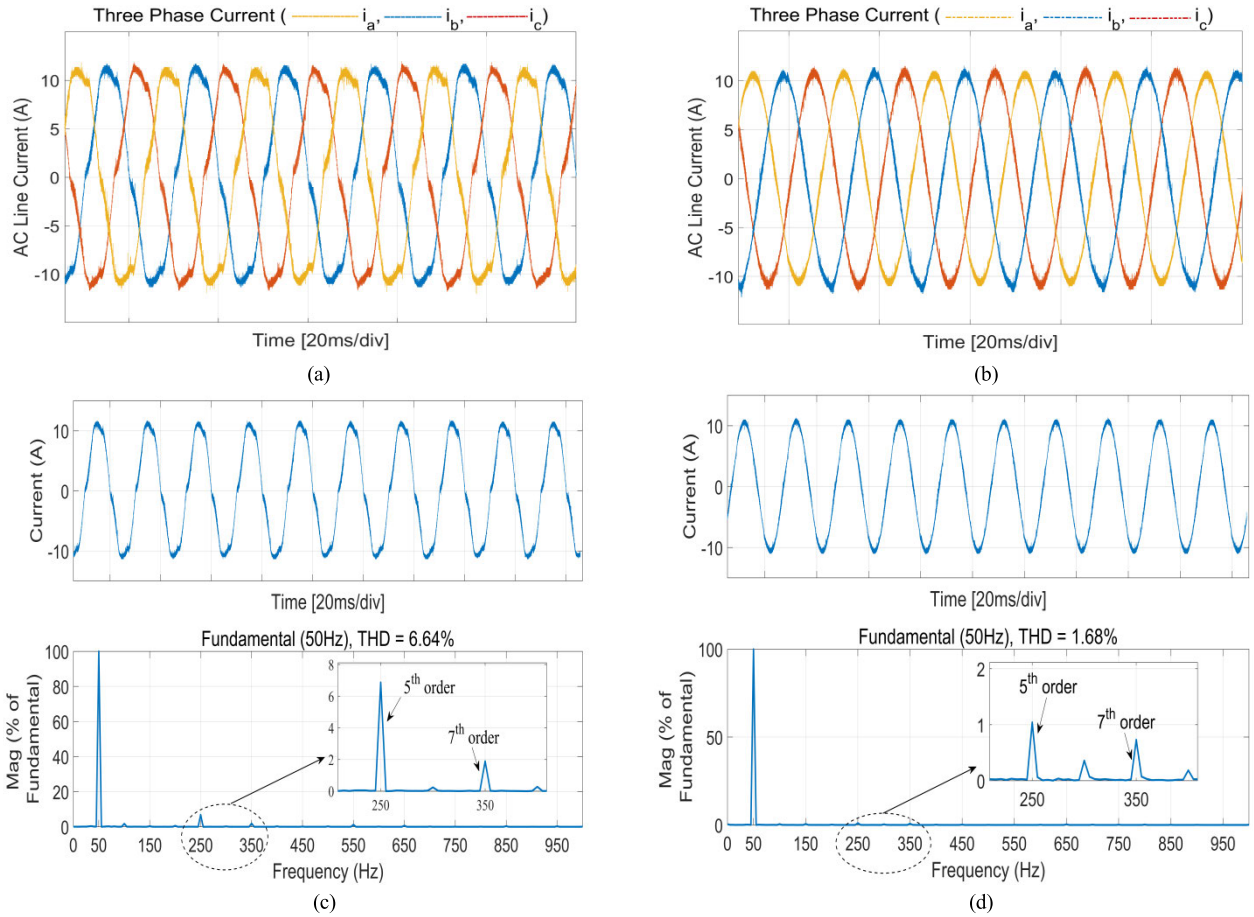

FIGURE 14. Experimental waveforms using optimized parameters based on emphasis factor $\gamma = 0.3$ (a) Three-phase current with PI controller alone (b) with PI-Repetitive controller (c)&(d) FFT analysis for THD measurement.

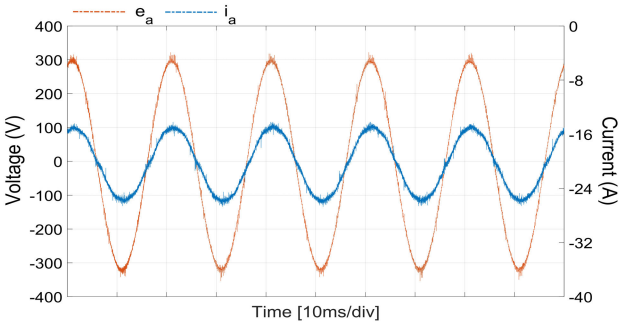

FIGURE 15. Power factor waveform for line current i_a and voltage e_a.

16.4, $K_{Pv} = 0.22$, and $K_{Iv} = 4.5$; optimized using (26) without repetitive control structure. The experimental result shows that with PI control alone, the %THD value is 6.64%.

Similarly, Fig. 14(b) and (d) show the experimental results with PI-RC. The results revealed that the harmonics are sufficiently reduced when PIR controller optimized values evaluated at $\gamma = 0.3$ are adopted. The simulated THD value is 1.82%, whereas the experimental THD is 1.68%. Moreover, the 5th and 7th order harmonics supremacy in the THD was demonstrated by 14(c) and (d). Although, results showed the percentage error between the simulated and experimental results. However, the simulation results are still very much consistent with the experimental results.

Fig. 15 shows that the unity power factor greater than 99% has also been achieved experimentally.

B. DYNAMIC PERFORMANCE INDICES ANALYSIS

Step load response from no load to full load i.e., $R_L = 98\Omega$ has been performed experimentally to verify the dynamic performance indices (E_{ss}, M_p, t_r, and t_s) as mentioned in Table 5. Fig. 16 illustrates the three-phase currents (i_a, i_b and i_c) behaviour during the step load transition from no load to full load at $t = t_1$ and a reverse step at $t = t_2$.

Fig. 17 shows the step load results using the optimized result with (a) $\gamma = 0.6$ (b) $\gamma = 0.3$. The experimental results for dynamic performance indices are consistent with the simulated results described in section VI-B.

Table 7 mentioned the % error between the simulated and experimental results. Although the % error is slightly higher for t_r and t_s; however, the absolute error is small among simulated and experimental results. Moreover, the experimental

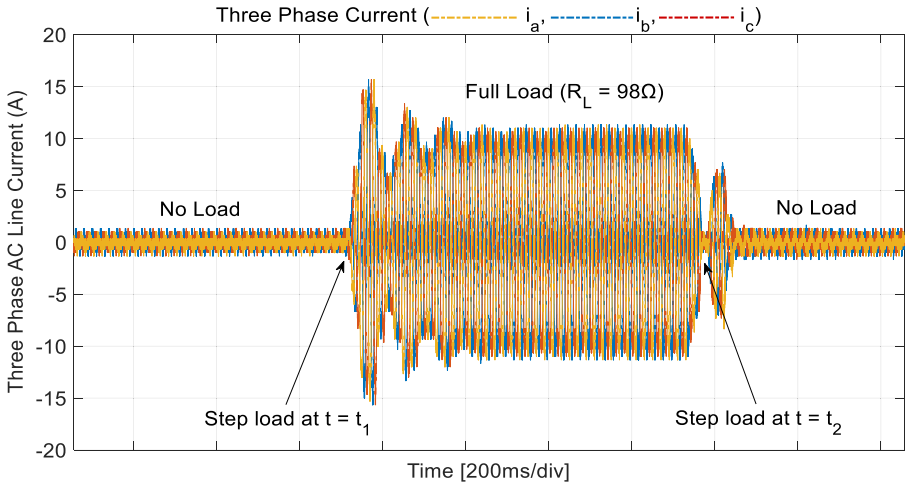

FIGURE 16. Step load voltage response of three-phase current for dynamic performance indices analysis.

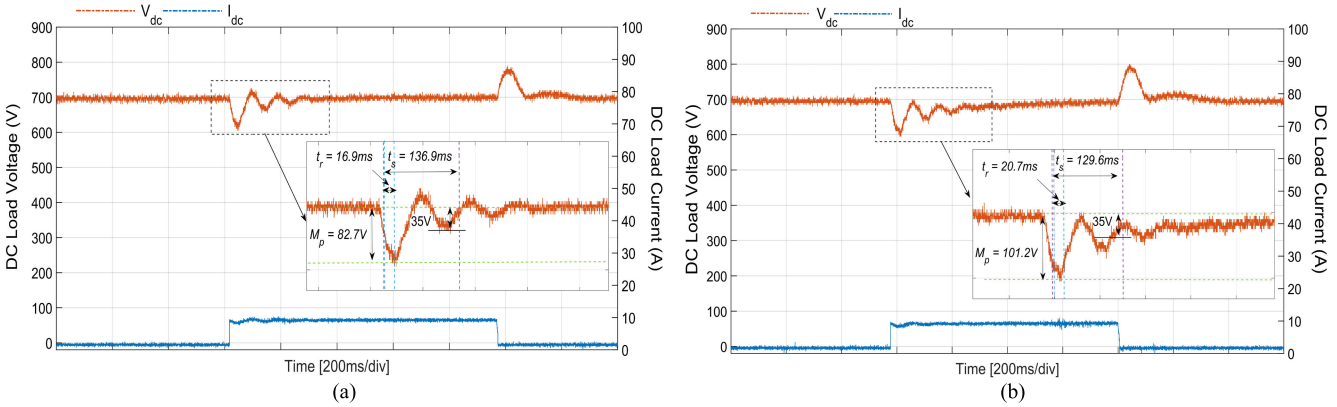

FIGURE 17. Load voltage V_o and load current I_o behavior during the step load change for dynamic performance indices evaluated (a) at $\gamma = 0.6$ (b) at $\gamma = 0.3$.

TABLE 7. Simulated and experimental results comparison.

Parameter	γ	Simulation Results	Experimental Results	% Error	Analysis
THD PI alone	0.3	7.09	6.64	6.3	THD
THD PI+RC		1.82	1.68	7.6	
M_p	0.3	110.8V	101.2V	8.6	Dynamic Performance Indices
t_r		17.0ms	20.7ms	17.8	
t_s		113.6ms	129.6ms	12.3	
M_p	0.6	74.27V	82.7V	10.2	
t_r		15.4ms	16.9ms	8.8	
t_s		134.4ms	136.9ms	1.8	
E_{ss}	0.3, 0.6	0	0	0	

results for THD show better performance compared with the simulated result, and this is because the exact discrete system simulation model cannot be readily achievable; hence, a small error always exists between the simulated and experimental results.

VIII. CONCLUSION

This paper presents a new objective function for combined PI and repetitive control parameters optimization using SGA for a three-phase boost PFC rectifier. Multiple simulation examples are performed based on different emphasis factors γ to

check the significance of the proposed objective function. Moreover, three-phase boost PFC rectifier performance is evaluated in terms of THD reduction and dynamic performance indices (M_p, E_{ss}, $t_{s,}$ and t_r) improvements using the separate evaluation functions. The proposed objective function is compared with existing objective functions, namely ISE, IAE, ITSE and ZLG. Simulation results demonstrated that our proposed objective function outperform existing objective functions to achieve optimized PI and RC parameter values. The improvement percentage of the proposed SGA-PIR controller for THD is 59.28% compared to ZLG at $\gamma = 0.3$. Similarly, the dynamic performance parameters such as M_p and t_r are improved by 13.03% and 2.53%, respectively, at the cost of higher settling time when $\gamma = 0.6$ is set.

The experiment results are performed on 5kW three-phase PFC rectifier with DSP TMS320F28335 prototype to validate the simulation results. Thus, the hardware results verified that using the SGA-PIR controller optimal values, THD has been reduced to 1.68% compared with the PI controller alone. Similarly, the percentage error between simulated and experimental results for the dynamic performance analysis (M_p, t_r, t_s, E_{ss}) evaluated at $\gamma = 0.3$ are 8.6, 17.8, 12.3 and 0, respectively; whereas at $\gamma = 0.6$, the values of dynamic performance indices are 10.2, 8.8, 1.8 and 0. Furthermore, it is revealed that the THD analysis evaluated at $\gamma = 0.3$ has shown better performance, whereas dynamic performance indices have superior results at $\gamma = 0.6$. Hence, based on different values of γ, there is a trade-off between %THD and dynamic performance indices.

The proposed SGA-PIR controller approach is evaluated under fixed loading conditions. However, the controller performance under different loading conditions have yet to be explored. The proposed solution can be adopted to optimize the multi-control loops parameters for various applications such as renewable energy systems, grid-connected power converters and electric vehicle battery charge systems etc.

ACKNOWLEDGMENT

The authors would also like to thank the Deanship of Scientific Research at Majmaah University, Saudi Arabia, for supporting this work.

REFERENCES

[1] H. Mao, D. Boroyevich, A. Ravindra, and F. C. Lee, "Analysis and design of high frequency three-phase boost rectifiers," in *Proc. IEEE Appl. Power Electron. Conf. (APEC)*, San Jose, CA, USA, Mar. 1996, pp. 538–544.

[2] Y. Ye, M. Kazerani, and V. H. Quintana, "Modeling, control and implementation of three-phase PWM converters," *IEEE Trans. Power Electron.*, vol. 18, no. 3, pp. 857–864, May 2003.

[3] Z. Zeng, X. Jin, and R. Zhao, "Small-signal discrete-time modeling of digitally controlled three-phase PWM boost rectifier under balanced voltage," *COMPEL-Int. J. Comput. Math. Electr. Electron. Eng.*, vol. 36, no. 1, pp. 18–47, Jan. 2017.

[4] J. W. Kolar and T. Friedli, "The essence of three-phase PFC rectifier systems—Part I," *IEEE Trans. Power Electron.*, vol. 28, no. 1, pp. 176–198, Jan. 2013.

[5] T. Friedli, M. Hartmann, and J. W. Kolar, "The essence of three-phase PFC rectifier systems—Part II," *IEEE Trans. Power Electron.*, vol. 29, no. 2, pp. 543–560, Feb. 2014.

[6] A. Kessal, L. Rahmani, J.-P. Gaubert, and M. Mostefai, "Experimental design of a fuzzy controller for improving power factor of boost rectifier," *Int. J. Electron.*, vol. 99, no. 12, pp. 1611–1621, Dec. 2012.

[7] A. Fekik, H. Denoun, N. Benamrouche, N. Benyahia, and M. Zaouia, "A fuzzy—Logic based controller for three phase PWM rectifier with voltage oriented control strategy," *Int. J. Circuits, Syst. Signal Process.*, vol. 9, pp. 412–419, Nov. 2016.

[8] M. Kissaoui, A. A. R. Al Tahir, A. Abouloifa, F. Z. Chaoui, Y. Abouelmahjoub, and F. Giri, "Output-feedback nonlinear adaptive control strategy of three-phase AC/DC boost power converter for on-line UPS systems," *IFAC-PapersOnLine*, vol. 49, no. 13, pp. 324–329, 2016.

[9] S. Ouchen, H. Steinhart, M. Benbouzid, F. Blaabjerg, and A. Betka, "Dynamic performance improvement of three phase shunt active power filter using predictive direct power control," in *Proc. 20th Eur. Conf. Power Electron. Appl. (EPE ECCE Eur.)*, Riga, Latvia, Sep. 2018, pp. 1–7.

[10] S. Gopalan, "A comparative study of control techniques for three phase PWM rectifier," in *Proc. 10th Int. Conf. Intell. Syst. Control (ISCO)*, Jan. 2016, pp. 1–8.

[11] A. Mallik and A. Khaligh, "Control of a three-phase boost PFC converter using a single DC-link voltage sensor," *IEEE Trans. Power Electron.*, vol. 32, no. 8, pp. 6481–6492, Aug. 2017.

[12] Q. N. Trinh, P. Wang, and F. H. Choo, "An improved control strategy of three-phase PWM rectifiers under input voltage distortions and DC-offset measurement errors," *IEEE J. Emerg. Sel. Topics Power Electron.*, vol. 5, no. 3, pp. 1164–1176, Sep. 2017.

[13] R. Guo and P. Qian, "Three-phase PFC control strategy based on fractional-order PID controller," *IOP Conf. Ser., Earth Environ. Sci.*, vol. 188, Oct. 2018, Art. no. 012047.

[14] M. A. Santoyo-Anaya, N. M. Salgado-Herrera, J. R. Rodriguez-Rodrıguez, L. M. Castro, E. L. Moreno-Goytia, and V. Venegas-Rebollar, "New phasorial oriented single-PI loop control for industrial VSC-PFC rectifiers operating under unbalanced conditions," *IET Power Electron.*, vol. 13, no. 4, pp. 844–853, Mar. 2020.

[15] K. Heong Ang, G. Chong, and Y. Li, "PID control system analysis, design, and technology," *IEEE Trans. Control Syst. Technol.*, vol. 13, no. 4, pp. 559–576, Jul. 2005.

[16] Š. Bucz and A. Kozáková, "Advanced methods of PID controller tuning for specified performance," in *PID Control for Industrial Processes*. London, U.K.: InTech, 2018, pp. 73–119.

[17] Y. Ma, X. Sun, and J. Chai, "Synchronous PI current control technique for three-phase PFC rectifier for PMSG wind generation system," in *Proc. 2nd Int. Symp. Power Electron. Distrib. Gener. Syst. (PEDG)*, 2010, pp. 236–239.

[18] S. Li, W. Lu, S. Yan, and Z. Zhao, "Improving dynamic performance of boost PFC converter using current-harmonic feedforward compensation in synchronous reference frame," *IEEE Trans. Ind. Electron.*, vol. 67, no. 6, pp. 4857–4866, Jun. 2020.

[19] X. H. Wu, S. K. Panda, and J. X. Xu, "Design of a plug-in repetitive control scheme for eliminating supply-side current harmonics of three-phase PWM boost rectifiers under generalized supply voltage conditions," *IEEE Trans. Power Electron.*, vol. 25, no. 7, pp. 1800–1810, Jul. 2010.

[20] L. He, K. Zhang, J. Xiong, and S. Fan, "A repetitive control scheme for harmonic suppression of circulating current in modular multilevel converters," *IEEE Trans. Power Electron.*, vol. 30, no. 1, pp. 471–481, Jan. 2015.

[21] G. A. R. Fuentes, J. A. C. Quintero, and I. D. M. Lagos, "High performance control of a three-phase PWM rectifier using odd harmonic high order repetitive control," *DYNA*, vol. 83, no. 198, pp. 27–36, Sep. 2016.

[22] W. Jian, W. Zhi-Qiang, L. Guo-Feng, W. Ning-Hui, and W. Jin-Jun, "PI-repetitive control applied to three-phase four-wire active power filter," in *Proc. 36th Chin. Control Conf. (CCC)*, Jul. 2017, pp. 10751–10756.

[23] M. S. Ali, L. Wang, and G. Chen, "Design and control aspect of segmented proportional integral-repetitive controller parameter optimization of the three-phase boost power factor correction rectifier," *Int. J. Circuit Theory Appl.*, vol. 49, no. 3, pp. 554–575, 2020.

[24] J. Honkanen, H. Jarvisalo, T. J. Karkkainen, and J. Korhonen, "Discussion of 'a comparative study between PI and type-II compensators for H-bridge PFC converter,'" *IEEE Trans. Ind. Appl.*, vol. 54, no. 4, p. 4009, Jul./Aug. 2018.

[25] K. Ogata, *Modern Control Engineering*, 4th ed. Upper Saddle River, NJ, USA: Prentice-Hall, 2002.

[26] E. I. Aniekan, O. Ikechukwu, and S. Paul, "Comparative analysis of a PID controller using Ziegler–Nichols and auto turning method," *Int. Academic J. Sci. Eng.*, vol. 6, no. 1, pp. 51–66, Jun. 2019.
[27] M. Liserre, A. Dell'Aquila, and F. Blaabjerg, "Genetic algorithm-based design of the active damping for an LCL-filter three-phase active rectifier," *IEEE Trans. Power Electron.*, vol. 19, no. 1, pp. 76–86, Jan. 2004.
[28] H. Peng Ren and T. Zheng, "Optimization design of power factor correction converter based on genetic algorithm," in *Proc. 4th Int. Conf. Genet. Evol. Comput. (ICGEC)*, Dec. 2010, pp. 293–296.
[29] N. Gowtham and S. Shankar, "PI tuning of shunt active filter using GA and PSO algorithm," in *Proc. 2nd Int. Conf. Adv. Electr., Electron., Inf., Commun. Bio-Inform. (AEEICB)*, Feb. 2016, pp. 207–213.
[30] M. S. Ali, L. Wang, and G. Chen, "Control system optimization of three-phase active rectifier based on evolutionary algorithm," in *Proc. 4th Int. Conf. Power Renew. Energy (ICPRE)*, Chengdu, China, Sep. 2019, pp. 212–216.
[31] S. Durgadevi and M. G. Umamaheswari, "Analysis and design of single-phase power factor corrector with genetic algorithm and adaptive neuro-fuzzy-based sliding mode controller using DC–DC SEPIC," *Neural Comput. Appl.*, vol. 31, no. 10, pp. 6129–6140, Oct. 2019.
[32] C. Komathi and M. G. Umamaheswari, "Analysis and design of genetic algorithm-based cascade control strategy for improving the dynamic performance of interleaved DC–DC SEPIC PFC converter," *Neural Comput. Appl.*, vol. 32, no. 9, pp. 5033–5047, May 2020.
[33] H. S. Krishnamoorthy, M. K. Vadali, and P. Supeda, "A novel, empirical equation—Based shunt active filter for harmonic elimination and power factor correction, using a modified PSO algorithm," in *Proc. Annu. IEEE India Conf. Eng. Sustain. Solutions (INDICON)*, Dec. 2011, pp. 1–5.
[34] X. Guo, H.-P. Ren, and D. Liu, "An optimized PI controller design for three phase PFC converters based on multi-objective chaotic particle swarm optimization," *J. Power Electron.*, vol. 16, no. 2, pp. 610–620, Mar. 2016.
[35] G. Tulay, İ. İskender, and H. Erdem, "Optimal tuning of a boost PFC converter PI controller using heuristic optimization methods," *Int. Trans. Electr. Energy Syst.*, vol. 27, no. 12, pp. 1–10, Dec. 2017.
[36] T. Eswaran and V. S. Kumar, "Particle swarm optimization (PSO)-based tuning technique for PI controller for management of a distributed static synchronous compensator (DSTATCOM) for improved dynamic response and power quality," *J. Appl. Res. Technol.*, vol. 15, no. 2, pp. 173–189, Apr. 2017.
[37] A. Rodríguez-Molina, E. Mezura-Montes, M. G. Villarreal-Cervantes, and M. Aldape-Pérez, "Multi-objective meta-heuristic optimization in intelligent control: A survey on the controller tuning problem," *Appl. Soft Comput.*, vol. 93, Aug. 2020, Art. no. 106342.
[38] K. Y. Lee and M. A. El-Sharkawi, *Modern Heuristic Optimization Techniques: Theory and Applications to Power Systems*. Hoboken, NJ, USA: Wiley, 2007.
[39] S. Mirjalili, "Genetic algorithm," in *Evolutionary Algorithms and Neural Networks*, vol. 780. Cham, Switzerland: Springer, 2019, pp. 43–55.
[40] S. Saremi, S. Mirjalili, and A. Lewis, "How important is a transfer function in discrete heuristic algorithms," *Neural Comput. Appl.*, vol. 26, no. 3, pp. 625–640, Apr. 2015.
[41] A. Ahmid, T.-M. Dao, and V. Lê, "Comparison study of discrete optimization problem using meta-heuristic approaches: A case study," *Int. J. Ind. Eng. Oper. Manage.*, vol. 01, no. 02, pp. 97–109, Dec. 2019.
[42] A. Y. Jaen-Cuellar, R. de J. Romero-Troncoso, L. Morales-Velazquez, and R. A. Osornio-Rios, "PID-controller tuning optimization with genetic algorithms in servo systems," *Int. J. Adv. Robot. Syst.*, vol. 10, no. 9, p. 324, Sep. 2013.
[43] S. Srivastava and V. S. Pandit, "Studies on PI/PID controllers in the proportional integral plane via different performance indices," in *Proc. IEEE 1st Int. Conf. Control, Meas. Instrum. (CMI)*, Jan. 2016, pp. 151–155.
[44] K. Jagatheesan, B. Anand, K. N. Dey, A. S. Ashour, and S. C. Satapathy, "Performance evaluation of objective functions in automatic generation control of thermal power system using ant colony optimization technique-designed proportional–integral–derivative controller," *Electr. Eng.*, vol. 100, no. 2, pp. 895–911, Jun. 2018.
[45] Z. Miao, T. Han, J. Dang, and M. Ju, "FOPI/PI controller parameters optimization using PSO with different performance criteria," in *Proc. IEEE 2nd Inf. Technol., Netw., Electron. Automat. Control Conf. (ITNEC)*, Chengdu, China, Dec. 2017, pp. 250–255.
[46] E. Çelik, "Incorporation of stochastic fractal search algorithm into efficient design of PID controller for an automatic voltage regulator," *Neural Comput. Appl.*, vol. 30, no. 6, pp. 1991–2002, 2018.
[47] B. Hekimoglu and S. Ekinci, "Grasshopper optimization algorithm for automatic voltage regulator system," in *Proc. 5th Int. Conf. Electr. Electron. Eng. (ICEEE)*, Istanbul, Turkey, May 2018, pp. 152–156.
[48] M. K. Habib and S. A. Ayankoso, "Modeling and control of a double inverted pendulum using LQR with parameter optimization through GA and PSO," in *Proc. 21st Int. Conf. Res. Educ. Mechatronics*, 2020, pp. 1–6.
[49] Z.-L. Gaing, "A particle swarm optimization approach for optimum design of PID controller in AVR system," *IEEE Trans. Energy Convers.*, vol. 19, no. 2, pp. 384–391, Jun. 2004.
[50] D. H. Kim, A. Abraham, and J. H. Cho, "A hybrid genetic algorithm and bacterial foraging approach for global optimization," *Inf. Sci.*, vol. 177, no. 18, pp. 3918–3937, Sep. 2007.
[51] C. Komathi and M. G. Umamaheswari, "Multi objective bacterial foraging optimization algorithm for power factor correction using interleaved DC–DC SEPIC converter," in *Proc. 9th Trends Ind. Meas. Automat. (TIMA)*, Jan. 2017, pp. 1–7.
[52] K. Eltag, M. S. Aslamx, and R. Ullah, "Dynamic stability enhancement using fuzzy PID control technology for power system," *Int. J. Control, Autom. Syst.*, vol. 17, no. 1, pp. 234–242, Jan. 2019.
[53] B. Hekimoğlu, "Sine-cosine algorithm-based optimization for automatic voltage regulator system," *Trans. Inst. Meas. Control*, vol. 41, no. 6, pp. 1761–1771, Apr. 2019.
[54] S. Ekinci and B. Hekimoglu, "Improved kidney-inspired algorithm approach for tuning of PID controller in AVR system," *IEEE Access*, vol. 7, pp. 39935–39947, 2019.
[55] P. K. Guchhait and A. Banerjee, "Stability enhancement of wind energy integrated hybrid system with the help of static synchronous compensator and symbiosis organisms search algorithm," *Protection Control Mod. Power Syst.*, vol. 5, no. 1, pp. 1–13, Dec. 2020.
[56] M. Malinowski, M. P. Kazmierkowski, and A. M. Trzynadlowski, "A comparative study of control techniques for PWM rectifiers in AC adjustable speed drives," *IEEE Trans. Power Electron.*, vol. 18, no. 6, pp. 1390–1396, Nov. 2003.
[57] C.-C. Hou, P.-T. Cheng, S. Bhattacharya, and J. Lin, "Modeling and control of three-phase active front-end converters," in *Proc. 33rd Annu. Conf. IEEE Ind. Electron. Soc. (IECON)*, Taipei, Taiwan, Nov. 2007, pp. 1449–1454.
[58] X. Yang, P. Liu, S. Xu, and S. Liu, "Analysis and design of a PMQR-type repetitive control scheme for grid-connected h6 inverters," *Appl. Sci.*, vol. 9, no. 6, p. 1198, Mar. 2019.
[59] N. S. Nise, *Nise's Control Systems Engineering*, 7th ed. Hoboken, NJ, USA: Wiley, 2017.
[60] *IEEE Recommended Practice and Requirements for Harmonic Control in Electric Power Systems*, IEEE Standard 519-2014, Jun. 2014.
[61] M. Liserre, F. Blaabjerg, and A. Dell'Aquila, "Step-by-step design procedure for a grid-connected three-phase PWM voltage source converter," *Int. J. Electron.*, vol. 91, no. 8, pp. 445–460, Aug. 2004.

MUHAMMAD SAQIB ALI was born in Rawalpindi, Pakistan, in 1981. He received the B.S. degree in electronics engineering from Hamdard University Karachi, Pakistan, in 2004, and the M.S. degree in electrical engineering and computer science from Seoul National University (SNU), South Korea, in 2010. He is currently pursuing the Ph.D. degree with the College of Electrical Engineering, Zhejiang University, China. Since 2004, he has been with the Faculty of the Electrical and Computer Engineering, COMSATS University (CUI), Pakistan. From 2007 to 2011, he was a Lecturer with CUI, and has been an Assistant Professor, since 2011. His current research interests include three phase AC/DC rectifier systems, wide band gap devices, parameters optimization using artificial intelligence techniques, space power systems, and photovoltaic power conditioning systems.

LEI WANG was born in Hunan, China, in 1995. He received the B.S. degree in electrical engineering from Chongqing University (CQU), Chongqing, in 2017. He is currently pursuing the M.S. degree with the College of Electrical Engineering, Zhejiang University, China. His research interests include EMC, motor driver, PFC, and cable modeling.

HANI ALQUHAYZ received the bachelor's degree in computer science and the master's degree in information systems management from King Saud University and the Ph.D. degree in computer science from De Montfort University, U.K. He is currently an Assistant Professor with the Computer Science Department, College of Science, Majmaah University, Saudi Arabia. He has authored several articles in high impacted journals, such as IEEE Access, *Sensors*, and *Wireless Communications and Mobile Computing*. His research interests include wireless security, scheduling, image processing, the IoT, security and privacy, data mining, machine learning, and artificial intelligence.

OBAID UR REHMAN was born in Islamabad, Pakistan, in 1987. He received the B.S. degree in electrical engineering from Riphah International University, Pakistan, and the M.S. degree from COMSATS University Islamabad, Pakistan, where he is currently pursuing the Ph.D. degree in electrical engineering. Since 2013, he has been a Lecturer with the Electrical and Computer Engineering Department, COMSATS University Islamabad. His research interests include power system planning, optimization, and control.

GUOZHU CHEN (Member, IEEE) was born in Hubei, China, in 1967. He received the B.S. degree in electrical engineering from Hangzhou Commerce University, Hangzhou, China, in 1988, and the M.S. and Ph.D. degrees in electrical engineering from Zhejiang University, Hangzhou, in 1992 and 2001, respectively. Since 1992, he has been with the faculty of the College of Electrical and Engineering, Zhejiang University. From 2000 to 2005, he was an Associate Professor with Zhejiang University, and has been a Professor, since 2005. From January 2001 to April 2004, he was a Visiting Scholar with the University of California at Irvine, Irvine, CA, USA. He holds more than 20 Chinese patents, and has contributed to more than 250 academic articles. His current research interests include high-power electronics applications and their digital control, active power quality control, such as APF, UPQC, SVC, dSTATCOM, and dFACTS, grid connection of renewable energy/distributed power generation, and power electronic system integration. In 2006, he was approved by the Chinese Education Ministry as the "New Century Excellent Talents in University." He has got of nine technical research awards, including the Second-Class S&T Progress Award of Ministry of Education, China, and the First-Class Research Achievement Award of Zhejiang Education Bureau.